Metal-to-insulator transition in sputter deposited 3Ni/Al thin films

H. P. Ng[a] and A. H. W. Ngan
Department of Mechanical Engineering, The University of Hong Kong, Pokfulam Road, Hong Kong, People's Republic of China

(Received 2 February 2000; accepted for publication 15 May 2000)

Thin films with a 3Ni/1Al atomic ratio were synthesized using low-power dc planar magnetron sputtering from a nickel–aluminum alloy target. Chemical analysis revealed that a significant amount of oxygen was incorporated into the Ni–Al thin films which were prepared under a typical vacuum of $\sim 1\times 10^{-5}$ mbar. These thin films were found to exhibit a prominent temperature dependence of electrical resistance, the magnitude of which diminishes upon increasing the film thickness or the *in situ* deposition temperature. Cross-sectional transmission electron microscopy revealed a nanocrystalline structure of the films which changes as a function of deposition temperature. Electron diffraction indicates the existence of a single-phase face-centered cubic structure in the nanocrystallites, yet with an enormous expansion of the crystal lattice for the low temperature deposited films when compared with the intermetallic Ni_3Al lattice. On raising the deposition temperature or increasing the film thickness, however, the lattice constant gradually declines toward the lattice constant of bulk Ni_3Al. An attempt is made to correlate the lattice structures of the crystallites and the electrical properties of the films with the potential influence of the dissolved oxygen in the Ni–Al lattice. © *2000 American Institute of Physics.* [S0021-8979(00)04316-4]

I. INTRODUCTION

As reviewed by Mott,[1] insulator-to-metal transition is quite common in disordered systems like amorphous metals and doped semiconductors, and in transitional metal oxides. Such transition behavior has also been identified in discontinuous metal films deposited on insulator substrates (e.g., Ref. 2). The materials studied within such context are mostly pure metals such as Pt, Au, Ni, and Pd deposited on nonconducting substrates like glass. By discontinuous films, it is meant that the film growth is in its very early stage, so that the deposited material is in the form of discrete islands. The typical thickness for this regime is a few to hundreds of Å. Such discontinuous film transition phenomenon has been reviewed extensively in monographs by, e.g., Chopra,[3] Coutts,[4] and Morris and Coutts.[5] The conduction mechanism is mostly interpreted in terms of tunneling and thermionic emission between islands, and is associated with an activation energy depending on the reciprocal of the island radius, so that the transition effect diminishes exponentially as the islands grow. The electrical transition is also known to be dependent upon an applied pressure, exhibiting the so-called piezoresistive effect. The electrical transition effect in discontinuous metal films is also sensitive to physical gaseous adsorption, and a potential application in this respect is as gas sensors.[6–8]

Intermetallic films are recently being studied as a new interest in terms of phase reaction and mechanical properties.[9–18] This is presumably because intermetallic compounds possess properties intermediate between those of metals and ceramics, and are therefore good candidate materials for protective coatings for metallic components. Two major groups of methods have been attempted to synthesize intermetallic films. The first is by physical vapor deposition (PVD) using multielement or alloy targets,[9,10,14,16–18] and the second is by phase reaction at multilayer interfaces.[11–13,15] The latter is more successful in producing more homogeneous phases but its applicability is system dependent. A few of the PVD reports were dedicated to the film structure and all of these concluded that the intermetallic-base films investigated had columnar structures. Many authors have implicitly assumed that the columns are grains and in fact this is predicted to be the case in single-element films by atomistic simulations.[19] Subcolumn nanostructural investigations are extremely rare, although Westra and Thomson[20] have discovered some subcolumnar, nanosized features in Ti–W films using atomic force microscopy. In Banerjee *et al.*'s work,[18] the formation and crystallization of amorphous phases in Ti–Al films deposited from alloy TiAl targets were reported. An anomalous structural allotropy effect exhibited by multilayers with nanosized bilayer thickness is also currently receiving much attention.[21]

In the course of a general program to investigate the fabrication and mechanical properties of Ni_3Al coatings on metallic substrates,[17] we have accidentally discovered that low-temperature sputter-deposited 3Ni/1Al films exhibit a rather surprising insulator-to-metal transition, the magnitude of which is adjustable by altering the deposition conditions. The purpose of this article is therefore to present this phenomenon and to elucidate its relationship with the observed microstructure of the films.

[a]Author to whom correspondence should be addressed; electronic mail: h9312914@hkusua.hku.hk

 © 2000 American Institute of Physics

Downloaded 05 Nov 2006 to 147.8.21.97. Redistribution subject to AIP license or copyright, see http://jap.aip.org/jap/copyright.jsp

II. EXPERIMENT

The nickel–aluminum thin films comprising 3Ni:1Al were fabricated using a dc planar magnetron sputtering device (Bal-Tec MED020) with a water-cooled Ni–27.4 at. %Al alloy target located 50 mm above the substrate stage. The sputtering vacuum chamber was evacuated to about 1×10^{-5} mbar prior to the injection of ultrahigh purity argon (over 99.9999%) at 2×10^{-2} mbar during operation. Presputtering of the target was performed for at least 60 min to thoroughly eliminate any surface oxides on the target prior to film deposition. High purity nickel (>99.5%) approximately 15 mm×20 mm×1 mm in size was used as substrates. The substrates were mechanically polished and solvent cleaned to remove organic contamination. The deposition temperature was controlled by a built-in heater which is capable of raising the substrate temperature up to 600 °C. The sputtering power was approximately 70 W and the corresponding deposition rate of the Ni–Al films was 2–3 Å/s. Film thickness was controlled by means of deposition time.

The film specimens for cross-sectional transmission electron microscopy (XTEM) were prepared by slicing a 3-mm-diam cylindrical assembly consisting of two deposited substrates glued together with their films facing against each other. The slices were mechanically polished to a thickness less than 80 μm, followed by twin-jet electropolishing with 90% methanol +10% perchloric acid at 5 V and −50 °C. All the XTEM specimens were examined using a JOEL 2000FX TEM operating at 200 kV.

The compositions of Ni–Al thin films were determined by a 20 kV Cambridge scanning electron microscope equipped with an Oxford energy dispersive x-ray (EDX) spectrometer. The crystal structure of the films was determined by selected area electron diffraction (SAD) in the TEM. X-ray diffraction (XRD) analysis of the film structure was also performed using a Siemens x-ray diffractometer with a Cu $K\alpha$ target operating at 40 kV/20 mA. A continuous scan from 20° to 80° with a resolution of 0.1° was performed for each XRD analysis.

The electrical resistance as a function of temperature was investigated for the Ni–Al thin films. The film resistance was probed by two flat copper electrodes that were fixed 5 mm apart and connected to a high accuracy digital ohmmeter (Tektronix DM257). The temperature of the films was monitored by a surface contact type thermocouple. The specimen was heated by a hot stage, the power of which was gradually controlled such that the samples were warmed up at a sufficiently low speed (typically less than 0.5 °C/s) to ensure quasisteady state conditions.

The current density–electric field ($J-E$) characteristics of the thin films were also measured. The deposited specimen was placed between two copper electrodes, each with an area of 0.78 cm^2, under a constant contact pressure of approximately 50 kPa. The potential difference across the film specimen was monitored by a voltmeter connected in parallel across both the specimen and a high accuracy ammeter.

TABLE I. Metallic compositions of the Ni–Al films.

Specimens deposited at different temperatures (°C)	Relative compositions of Ni–Al thin films (at. %±0.5%)	
	Ni	Al
100	74.0	26.0
300	74.4	25.6
500	74.6	25.4

III. RESULTS

A. Composition and microstructure of the Ni–Al films

Quantitative EDX analyses were performed to measure the relative abundance of nickel and aluminum in the sputtered Ni–Al thin films. The EDX results in Table I show that the Ni and Al compositions of the films essentially comply with the range over which the intermetallic Ni_3Al compound would exist. Apart from nickel and aluminum, however, a noticeable amount of oxygen was also detected in the films. Figure 1 illustrates the energy spectra collected from the surfaces of two Ni–Al films with unlike thicknesses deposited on Ni substrates under similar operating conditions. The spectrum of the thinner film (250 nm) consists of much higher nickel peaks than the thicker film (1 μm), suggesting that in the former the excitation volume of the electron beam has already penetrated into the pure nickel substrate. The relative oxygen content of the film is better assessed by reference to the aluminum peak. By comparing the areas under the peaks after subtracting the background signal, it is found that the O_k peak grew as the film thickness increased, but the ratio of the O_k peak to that of the Al_k peak decreased from 4.22 for the thinner film to 2.50 for the thicker film. This suggests that although oxygen was incorporated in the film at

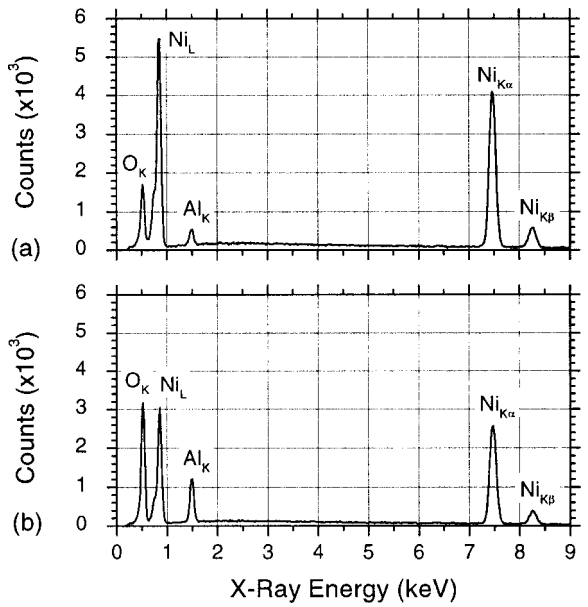

FIG. 1. EDX spectra collected from: (a) a 250 nm thick and (b) a 1 μm thick 3Ni/1Al films sputter deposited at 300 °C on pure nickel, showing the increase of the O peak amplitude with the film thickness.

Downloaded 05 Nov 2006 to 147.8.21.97. Redistribution subject to AIP license or copyright, see http://jap.aip.org/jap/copyright.jsp

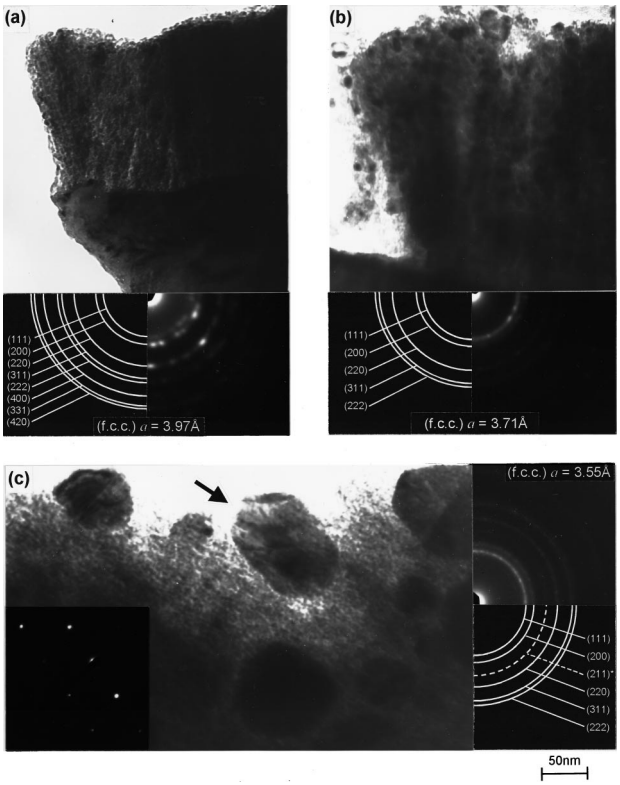

FIG. 2. XTEM micrographs showing the nanostructures and SAD patterns of 3Ni/1Al thin films deposited *in situ* at: (a) 100 °C, (b) 300 °C, and (c) 500 °C on Ni substrates. Note that the lattice parameter of the film matrix decreases with increasing deposition temperature. The SAD pattern shown on the bottom-left corner of (c) corresponds to the big crystal as arrowed.

a fairly steady rate during the deposition process, the thinner film nevertheless contained a relatively higher oxygen content.

The microstructure of the sputter-deposited nickel–aluminum films was investigated using XTEM. Comparison of the cross-sectional morphologies in Fig. 2 clearly demonstrates a structural transformation of the thin films as the deposition temperature increases. A pronounced columnar texture is noted in the low temperature deposited specimens. The constitution of individual columns can be observed to be an aggregate of extremely fine crystallites with a size of a few nm. As the deposition temperature increases, the crystals grow rapidly and meanwhile a higher structural continuity is achieved. This is well illustrated in the 500 °C specimen, which contains some crystals with size over 100 nm and shows hardly any columnar boundaries.

TABLE II. Crystallographic structures determined for thin (by SAD) and thick (by XRD) 3Ni/1Al films. Note the lattice expansion at decreasing film thickness and deposition temperatures.

Deposition temperature (°C)	Crystallographic structures of Ni–Al films		
		Lattice constant (a)	
	Lattice structure	Thin (<1 μm)	Thick (>5 μm)
100	fcc	3.97	3.601
300	fcc	3.71	3.577
500	fcc	3.55	3.562

The crystallite lattice structure is also characterized by the SAD patterns shown alongside the XTEM micrographs in Fig. 2. It is evident for all the specimens that the constituent crystallites exhibit fundamental reflections of a face-centered cubic (fcc) lattice. The measured lattice constant a for respective XTEM specimens, together with a set of data obtained for another batch of thick films by XRD, are tabulated in Table II. It can be seen that the lattice constant of the identified fcc phase is not constant but undergoes a progressive increase as the deposition temperature or the film thickness decreases. For films thinner than 1 μm, the fcc lattice constant is noted to decline from slightly below 4 Å at 100 °C to 3.55 Å at 500 °C. Apparently no known phases of the Ni–Al–O ternary system have been found to possess a fcc structure with lattice constant lying within such an observed range (Table III), but there is a clear tendency for the observed lattice constant to approach that of the nickel-rich γ phase (3.52 Å) or the Ni_3Al γ' phase (3.57 Å) at large film thickness or high deposition temperatures. Moreover, as observed in the SAD pattern of the 500 °C XTEM specimen, there exists a relatively weak ring inbetween the (200) and (220) reflections, which can be indexed as the (211) superlattice reflection corresponding to the ordered Ni_3Al. Although similar superlattice reflections are not visible in the SAD patterns of the larger crystals embedded in the same specimen, they are found to possess a lattice constant even closer to the Ni_3Al phase. The establishment of ordered Ni_3Al at high temperatures in thick films has been confirmed by *postmortem* annealing. Figure 3 shows the XRD traces obtained from Ni–Al films *postmortem* heat treated in a vacuum of 1×10^{-6} Torr. The spectrum for the 700 °C specimen clearly shows two minor peaks corresponding to the superlattice (100) and (110) reflections of γ'-Ni_3Al.

TABLE III. Crystallographic data of the known phases in the Ni–Al–O system[a].

Phase Pearson symbol	(Al) cF4 (Cu)	γ(Ni) cF4 (Cu)	$NiAl_3$ oP16	Ni_2Al_3 hP5	NiAl cP2 (CsCl)	Ni_5Al_3 oC16	γ' Ni_3Al cP4 ($AuCu_3$)	Al_2O_3 hR30	NiO(h) cF8 (NaCl)	NiO(r) hR?	$NiAl_2O_4$ cF56 (spinel)
Lattice parameters (Å)	$a=4.05$	$a=3.52$	$a=6.61$ $b=7.37$ $c=4.81$	$a=4.04$ $c=4.90$	$a=2.89$	$a=7.44$ $b=6.68$ $c=3.72$	$a=3.57$	$a=4.75$ $c=12.99$	$a=4.18$	$a=4.18$	$a=7.95-8.05$

[a]See Ref. 22.

Downloaded 05 Nov 2006 to 147.8.21.97. Redistribution subject to AIP license or copyright, see http://jap.aip.org/jap/copyright.jsp

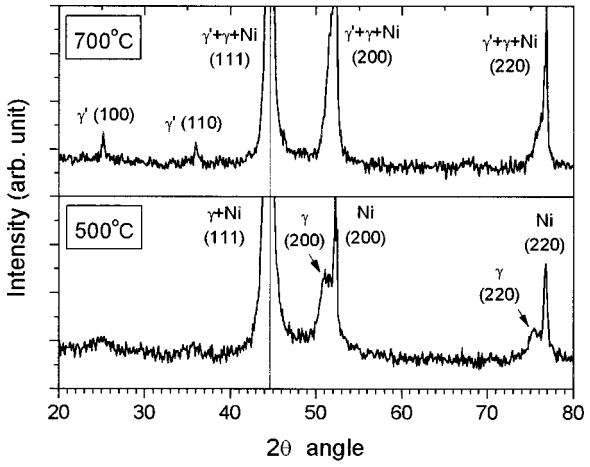

FIG. 3. X-ray diffraction patterns of 3Ni/1Al thin films deposited on Ni substrates without substrate heating and *postmortem* annealed in ultrahigh vacuum, respectively, at 500 °C (lower) and 700 °C (upper) for 2 h. The Ni peaks correspond to the substrates. Note the emergence of two superlattice reflections of γ' after 700 °C annealing.

B. Electrical behavior of the Ni–Al films

The electrical resistance of the freshly deposited Ni–Al thin films is found to be abnormally high at room temperature. An investigation into the resistance–temperature behavior of a 100 °C deposited Ni–Al thin film (~100 nm thick) was performed. Figure 4 illustrates that the resistance of the as-deposited film declines rapidly from a high value immeasurable by our meter ($\geqslant$20 MΩ) down to several hundred kΩ as temperature increases from room temperature to about 200 °C. Upon repeated heating and cooling, the resistance–temperature relation first underwent a hysteresis but its magnitude declined as more heating–cooling cycles were spent, finally achieving complete reversibility in the resistance change at steady state. A control experiment was performed to deposit a pure nickel film of a similar thickness onto pure nickel substrate and normal metallic behavior was found over the same temperature range (Fig. 4). 3Ni/1Al films deposited at low temperatures on glass and stainless steel substrates were also found to exhibit similar insulator-to-metal transition as in Fig. 4. These indicate that the transition is a specific effect for the 3Ni/1Al films and is substrate independent.

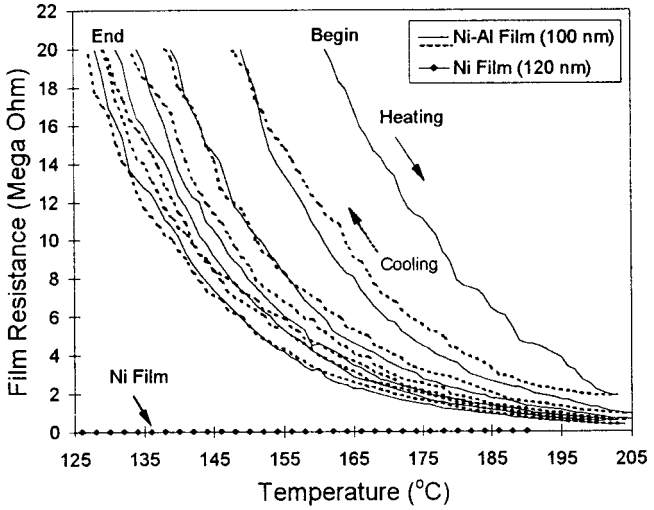

FIG. 4. Typical variation of the electrical resistance as a function of temperature of the 100 °C deposited Ni–Al thin films during a series of heating-and-cooling processes, together with that of a pure Ni film as a comparison.

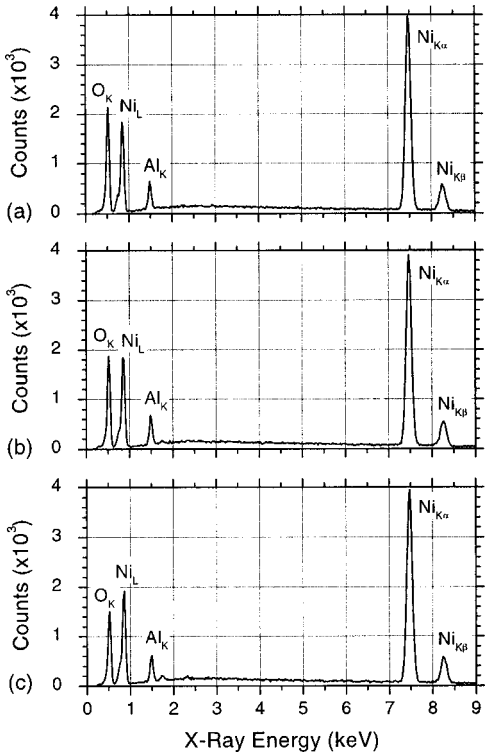

FIG. 5. EDX spectra collected from 100 °C deposited 330 nm thick 3Ni/1Al films: (a) as deposited, *postmortem* high vacuum (approximately 1×10^{-6} Torr) annealed for 5 h at (b) 300 °C and (c) 500 °C, respectively.

The effects of *postmortem* annealing at elevated temperatures on the 100 °C deposited films in high vacuum (approximately 1×10^{-6} Torr) were also investigated. Here all the films had the same thickness of 330 nm. Figure 5 shows the result of an EDX analysis for individual specimens, from which it can be seen that while the relative ratio of Ni to Al remains constant after annealing, there appears to be a progressive reduction in the oxygen content in the film after annealing at 300 and 500 °C (see Table IV). Figure 6 shows the *steady-state* resistance–temperature relations for the as-

TABLE IV. Comparison of the EDX peak ratios measured from sputter-deposited 3Ni/1Al thin films under various processing conditions. The ratios are determined according to the areas under the K peaks of the respective elements in the EDX spectra. The error of O peak is about ±2% and those of Ni and Al peaks are ±0.5% for each specimen. Note the progressive decline of the O:Al ratio with increasing annealing temperatures or decreasing film thickness.

	330 nm thick 3Ni/1Al films *postmortem* vacuum annealed at:			300 °C as-deposited 3Ni/1Al films with thicknesses of:	
Specimens	100 °C	300 °C	500 °C	250 nm	~1 μm
O:Al	3.89	3.43	2.85	4.22	2.50
Ni:Al	14.72	14.22	14.59	17.22	3.67

Downloaded 05 Nov 2006 to 147.8.21.97. Redistribution subject to AIP license or copyright, see http://jap.aip.org/jap/copyright.jsp

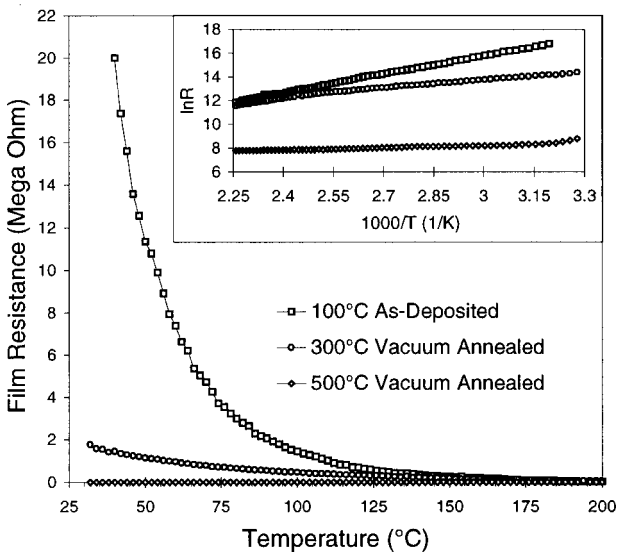

FIG. 6. The steady state resistance–temperature relationship for the 100 °C as-deposited and *postmortem* heat-treated 3Ni/1Al films (330 nm). The inset $\ln R$–$1/T$ plot indicates the film conduction mechanism follows an Arrhenius rate process.

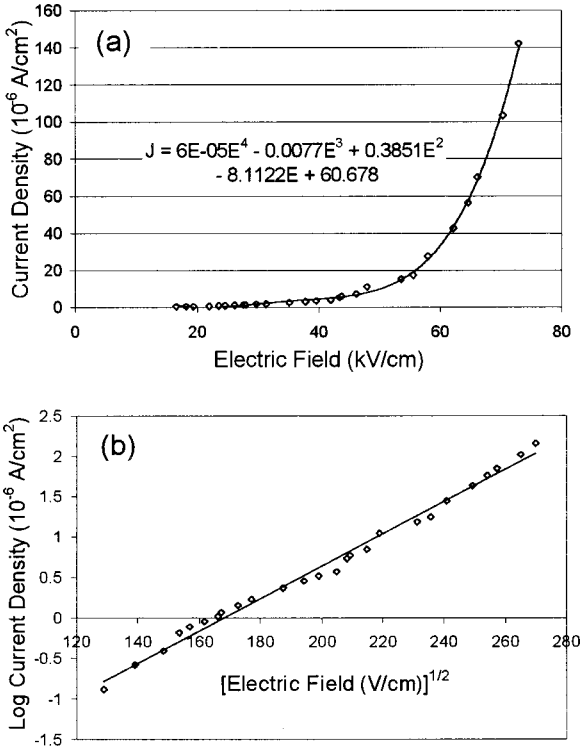

FIG. 7. (a) Typical J–E characteristics of the low temperature deposited Ni–Al thin films, and (b) the corresponding log J vs $E^{1/2}$ plot.

deposited and the annealed films. It can be seen that, with *postmortem* annealing, the overall resistance drops progressively, and the steady-state temperature dependence of the resistance gradually diminishes until the Ni–Al films approximate metallic conduction characteristics upon annealing at 500 °C. The linear plot of the logarithm of resistance ($\ln R$) as a function of the reciprocal of temperature ($1/T$) in Fig. 6 suggests that the conductivity obeys an Arrhenius law, with the activation energy E_a declining from the as-deposited value of 0.43–0.05 eV after annealing at 500 °C (Table Va).

Increasing the film thickness has also been found to have a similar effect as annealing Table Vb summarizes the variation of the activation energy as the thickness increases from ~100 nm to over 1 μm, which clearly indicates that the insulating behavior of the film diminishes as thickness increases.

Figure 7(a) shows the J–E characteristics of a thin Ni–Al film. It resembles that of a semiconductor diode, yet with a much higher current density level. The J vs E curve can be represented by a polynomial of the fourth order, which is likely to represent a space-charge-limited emission mechanism of electrical conduction.[23] A fairly linear relationship obtained in the log J vs $E^{1/2}$ plot in Fig. 7(b), on the other hand, suggests that the Poole–Frenkel thermionic emission mechanism might also be important in the electrical transport in the films.[24,25]

TABLE V. Conduction activation energies of (a) 330 nm thick films deposited at 100 °C followed by *postmortem* annealing and (b) of films deposited at 100 °C with various thicknesses.

(a) Annealing temperature	As-deposited		300 °C	500 °C
E_a (eV)		0.43	0.20	0.05
(b) Thickness (nm)	100	120	330	1100
E_a (eV)	0.83	0.76	0.43	≈0

IV. DISCUSSION

The transition observed here in the Ni–Al films appears to be distinct from those discovered in other systems in the following aspects:

(i) From a structural viewpoint, the Ni–Al films exhibiting the electrical transition are in the ''continuous'' regime with thickness in hundreds of nm. This is two to three orders of magnitude thicker than the discontinuous island regime,[3–5] and the substrate is totally covered by the deposited material. The subcolumnar nanocrystallite structure of the Ni–Al films is also more complex than the islands in the discontinuous film.

(ii) The transition in Ni–Al films is very sharp with activation energies a fraction of an eV. The transitions observed in discontinuous metal films are more gentle except for films with Angstrom-sized islands. The transitions observed in films of semiconducting materials are also more gentle.[26]

(iii) The electrical behavior of the Ni–Al films, in terms of activation energy and amplitude, is rather similar to bulk transitional-metal oxides,[27] but the effect in Ni–Al films disappears at large film thickness.

One of the interesting features of the sputter-deposited Ni–Al thin films is the significant incorporation of oxygen as shown in Figs. 1 and 5. The incorporated oxygen will not

Downloaded 05 Nov 2006 to 147.8.21.97. Redistribution subject to AIP license or copyright, see http://jap.aip.org/jap/copyright.jsp

only relate to the observed metal-to-insulator transition as will be discussed later, but may well retard the crystallization and ordering of the 3Ni/Al alloy. It is generally regarded that gas is more likely to be entrapped in a relatively amorphous medium than in a crystalline state.[28] Under a base vacuum of 1×10^{-5} mbar and a slow deposition rate adopted in the present film fabrication process, a significant amount of oxygen is expected to be implanted into the Ni–Al matrix. It has been previously reported that 800 °C was required to crystallize an originally amorphous Ti–Al thin film which contained 6 at. % oxygen, whereas 430 °C would be sufficient to obtain the ordered TiAl intermetallic compound from one with 1 at. % oxygen.[29] This seems to imply that oxygen has a tendency to retain the disordered structure of the intermetallic thin films until sufficient thermal energy is supplied. In line with this, the XRD results in Fig. 3 show that Ni_3Al evolves from the Ni–Al matrix at a temperature between 500 and 700 °C, which is a value comparatively higher than those reported elsewhere.[10,13,30] The retardation of the ordering of γ is therefore thought to be due to the dissolved oxygen in the metallic matrix.

The key question is in what form does the dissolved oxygen exist in the alloy film. Little is known about the Ni–Al–O equilibrium phase diagram below 900 °C, but between 900 and 1000 °C, previous studies[22] have shown no extended phases between Ni_xAl_{1-x} and O. Instead, all the phases in the Ni–Al binary system are found to coexist with one or more of the three stable oxide phases: Al_2O_3, NiO, and the spinel $NiAl_2O_4$. If equilibrium is assumed in our experiment, one might therefore expect that one or more of these oxide phases will coexist with the metallic phases of ordered γ'-Ni_3Al or disordered γ. These oxide phases may exist in several forms, namely, as precipitates dispersed within the metallic matrix, as segregation along columnar boundaries, or as thin oxide layers enclosing each of the observed nanosized, subcolumnar grains. However, our XRD and TEM/SAD experiments failed to detect any crystalline forms of these oxide phases. The fairly stable $NiAl_2O_4$ phase bears a spinel fcc derivative structure (cF56), but the drastic difference between its lattice constant (~8 Å) and those measured for the fcc structures of the low-temperature deposited Ni–Al films (~4–3.7 Å) suggests that these structures were not the $NiAl_2O_4$ phase. Similarly, the existence of the cF8 NiO and the hR30 Al_2O_3 can be ruled out. It seems therefore unlikely that oxygen would exist in the form of crystalline oxide precipitates or segregation along grain boundaries.

There might still be two other possibilities. The first is the existence of amorphous oxide precipitates or segregation, and the second is thin oxide layers (amorphous or crystalline) enclosing the nanosized, subcolumnar grains. It has been found that it is quite common for thin oxide layers to form on the surface of nanosized metal powders.[31] It is therefore quite possible that similar oxide layers may develop on the fine crystallites in our case during deposition. Yet, these layers are usually very thin (only a few monolayers thick), so that they may not be easily detectable by XRD or TEM/SAD even when they are crystalline. To reveal the existence of these oxide layers would require high resolution electron microscopy but because the crystallites in our case are not isolated as in the powder situation and also their sizes are as small, this would be a very difficult task. On the other hand, we also notice that the lattice size observed by TEM/SAD is about 11% enlarged at low temperatures but it drops toward the equilibrium γ or γ' value at higher temperatures or film thickness. Hence, even though amorphous oxide phases or thin oxide layers on crystallites may exist, something must have occurred to the metallic phase itself to cause it to expand by 11% or so. It is interesting to note that the present observed expansion in lattice is not unique, as an early work of Chopra *et al.*[3,32] has also shown that a wide range of fcc transitional metals exhibit an increase in atomic volume when they are prepared in thin film forms. Very obviously, such a lattice expansion cannot be explained by residual or mismatch stresses between the oxide and the metallic phases, because the stress required to produce a volumetric strain of 11% in the present case would be too large to be realistic. Moreover, the three oxide phases of Ni and Al are all very stable. They should not easily decompose upon moderate heating at a temperature of about 500 °C, at which the lattice constant of nickel rich γ has already been restored. The conclusion therefore is that one cannot interpret the incorporated oxygen content and the enormous lattice expansion by simply referring to the equilibrium oxide phases of the Ni–Al–O system. Some nonequilibrium phenomena must have taken place.

The main support of the nonequilibrium argument, however, is that the lattice constant is found to decrease not only with increase in temperature but also with increase in film thickness (Table II). This rules out that the observed variations in lattice constant are due to an equilibrium phase transformation effect, since if it were the case, the changes would have been thickness or volume independent. In view of the progressive reduction of the lattice size toward that of Ni_3Al upon increasing temperature or thickness, we speculate here that the low-temperature film structures are actually a series of expanded disordered nickel rich (γ) lattices, from which oxygen is progressively expelled at higher temperatures to form the more stable γ'-Ni_3Al. Oxygen has an atomic radius of about 0.5–0.7 nm as reported by different sources,[33,34] while those of Ni and Al are, respectively, 1.25 and 1.43 nm. This size factor seems favorable for oxygen to be accommodated interstitially inside the Ni–Al lattice. Assuming an ideal atomic model in which oxygen is situated perfectly at the interstitial sites of a Ni_3Al unit cell, an increment as high as 9% in the Ni_3Al lattice size can be deduced from the above atomic radii. This argument is therefore capable of explaining the 11% lattice expansion as observed in the low-temperature deposited specimens. Owing to this extensive volume expansion, such a crystal configuration is presumably highly unfavorable in thermodynamic terms. Stability can be regained by expelling the interstitial oxygen atoms out of the matrix when more equilibrium conditions are established at higher temperatures. A process like this would be especially enhanced in the case when the crystal sizes are small. The crystallites in our 3Ni/1Al films are in general smaller than 10 nm at low deposition temperatures, which represent a few tens of monolayers. The migration of

Downloaded 05 Nov 2006 to 147.8.21.97. Redistribution subject to AIP license or copyright, see http://jap.aip.org/jap/copyright.jsp

oxygen should be reasonably efficient at moderate annealing temperatures. This is one possible reason for the loss of oxygen in the films after *postmortem* annealing as indicated in Fig. 5. Still, a noticeable level of oxygen remained in the 3Ni/1Al films even after the normal Ni–Al lattice size has been restored at 500 °C. This may be due to oxide layers along the boundaries between crystallites or between columns in the columnar microstructure. At a constant deposition temperature and hence state of the film, increasing the film thickness would increase proportionately any excess energy due to nonequilibrium conditions. Given the same degree of oxygen supersaturation, a thicker film would therefore have a higher driving force to expel the excessive oxygen than a thinner film. This would explain the restoring of the bulk γ or γ' lattice constant (Table II) and the loss of oxygen content (Table IV) as the film thickness increases.

The next problem to consider is the origin of the observed electrical transition from the insulating to the metallic state. In discussing this, it is useful to distinguish the *reversible* transition observed upon mild heating of the as-deposited state up to, say, 200 °C (Fig. 4) from the *permanent* resumption of the metallic behavior upon increasing the film thickness or upon strong heating at, say, 500 °C (Table V). The former has to be due to either some reversible structural change in the film, or if this is not the case, an intrinsic electronic activation process. The permanent transition to the metallic state, however, must be due to a permanent structural change of the film. For the reversible transition, one possible cause for a reversible structural change may be due to thermal stresses. There may be a thermal mismatch effect which causes the columnar gaps to close up when the film is heated and to open up when cooled. This may occur when the film material has a higher expansivity than the substrate. Closure of the gaps upon heating may then lead to improved conduction, and vice versa upon cooling. However, this mechanism cannot explain the Arrhenius rate law dependence of resistance change with temperature as observed in Fig. 6. If the gaps are the barriers to conduction, the activation energy should then depend on the gap width[8] and this, in the thermal mismatch mechanism, should decrease with increasing temperature and vice versa. The fact that the observed activation energy is a constant contradicts this. There may also be the possibility that the temperature change alone or the associated thermal stresses may trigger off some form of diffusional or diffusionless transformation of the film crystal structure but such a possibility is very remote as the observed resistance changes in the reversible regime are continuous and reversible.

We therefore believe that the reversible transition is not caused by a reversible structural change but is instead a consequence of an electronic activation process. Given the complexity of the observed film nanostructure, there may be a number of plausible explanations for the occurrence of such an activation process. One possible explanation is that the columnar gaps and oxide layers along these gaps or along subcolumnar crystallite boundaries may form places of poor conduction. If the structures of these barriers do not change with temperature, then pushing electrons through them would require a characteristic constant activation energy and hence the Arrehnius dependence of the resistance change can be explained. At larger film thickness or after postdeposition annealing at a moderate temperature, the columnar boundaries were observed to become more diffuse and the subcolumnar crystallites coalesce. There is therefore the possibility that these structural changes may reduce the number and width of the columnar gaps, thus causing a permanent transition to the metallic state. The oxide layers may also be broken up by the structural changes, but as Ni and Al oxides are very stable they should then remain in the lattice of the coalesced crystals. Thus whether they would contribute to the permanent transition is not clear.

Another plausible explanation for the electrical transition is due to the trapped oxygen within the lattice and the associated lattice expansion. Figure 6 and Table V indicate clearly that the activation energy for conduction gradually diminished after postdeposition annealing at increasing temperatures or at increasing film thickness. Tables II and IV indicate that under these conditions, the lattice constant dropped back to the equilibrium γ' value and the oxygen content decreased. It thus appears that there is a one-to-one correspondence between the activation energy for conduction and the lattice parameter or oxygen content. In band-crossing transition theories attributed originally to Mott,[1] metallic behavior would be produced out of an originally insulating behavior when the composition or lattice dimension of the material changes to an extent to cause an overlap of the valance and conduction bands. The observed increasing oxygen content and lattice expansion of the films at lower deposition temperatures may quite likely cause band overlap to disappear, which would then explain the associated insulating behavior. At low heating temperatures below, say, 200 °C (Fig. 4), oxygen will still remain in the lattice and the band gap would still persist, but electrons can be promoted across the band gap and the conduction would follow an Arrehnius law with the band gap being the activation energy. On the other hand, the large supersaturated amount of oxygen in the crystal lattice would represent frequent local fluctuations of the crystal potential. These oxygen sites may become potential sites to localize electron waves according to the Anderson localization theory.[1] The localized states, which occur in the vicinity of the extremities of the energy band, would inactivate the carriers and would result in a reduced conductivity of the material. Transfer from one localized state to another can still take place via thermally activated hopping. This mechanism would be consistent with the thermionic emission characteristics apparent in Fig. 7. When oxygen is expelled out of the lattice by heating or increasing the film thickness, the local disorder of the crystal potential diminishes and hence electrical conduction would become easier.

If the effects of oxygen postulated here are correct, the transition effect of the Ni–Al films should disappear as the base pressure decreases. It would thus be interesting as future work to investigate the effect of base pressure. Since the magnitude of the transition here is changeable according to the deposition conditions, a potential use of the effect here would be as thin film thermistors,[27] which may find applications in microelectromechanical systems.

Downloaded 05 Nov 2006 to 147.8.21.97. Redistribution subject to AIP license or copyright, see http://jap.aip.org/jap/copyright.jsp

V. CONCLUSIONS

A novel insulator-to-metal transition effect has been discovered for 3Ni/1Al thin films sputter deposited at low temperatures. Such an effect may be attributed to an observed significant amount of dissolved oxygen in these films. The film structure consists of nanosized fcc crystallites whose lattice constant is enlarged, presumably by the dissolved oxygen, up to about 10% compared with the bulk γ or γ' value at low deposition temperatures and small thickness.

ACKNOWLEDGMENTS

The present research was supported by a CRCG grant from the University of Hong Kong (Project No. 10202005/16180/14500/301/01). Stimulating discussions with Dr. K. K. Fung of HKUST are also gratefully acknowledged.

[1] N. F. Mott, *Metal-Insulator Transitions* (Taylor & Francis, London, 1990).
[2] C. A. Neugebauer and M. B. Webb, J. Appl. Phys. **34**, 74 (1963).
[3] K. L. Chopra, *Thin Film Phenomena* (McGraw–Hill, New York, 1969).
[4] T. J. Coutts, *Electrical Conduction in Thin Metal Films* (Elsevier, Amsterdam, 1974).
[5] J. E. Morris and T. J. Coutts, Thin Solid Films **47**, 3 (1977).
[6] A. Barr, Thin Solid Films **41**, 217 (1977).
[7] J. E. Morris and F. Wu, Thin Solid Films **246**, 620 (1994).
[8] J. E. Morris, A. Kiesow, M. Hong, and F. Wu, Int. J. Electron. **81**, 441 (1996).
[9] Y. Ding, Y. Zhang, D. O. Northwood, and A. T. Alpas, Surf. Coat. Technol. **94–95**, 483 (1997).
[10] R. K. Singh, D. Bhattacharya, S. Sharan, P. Tiwari, and J. Narayan, J. Mater. Res. **7**, 2639 (1992).
[11] E. Ma, M.-A. Nicolet, and M. Nathan, J. Appl. Phys. **65**, 2703 (1989).
[12] L. S. Hung, M. Nastasi, J. Gyulai, and J. W. Mayer, Appl. Phys. Lett. **42**, 672 (1983).
[13] A. Zalar, S. Hofmann, D. Kohl, and P. Panjan, Thin Solid Films **270**, 341 (1995).
[14] R. G. Rowe and D. W. Skelly, Mater. Res. Soc. Symp. Proc. **273**, 411 (1992).
[15] K. Barmak, C. Michaelsen, R. Bormann, and G. Lucadamo, Mater. Res. Soc. Symp. Proc. **382**, 33 (1995).
[16] T. Suzuki, H. Umehara, and R. Hayashi, J. Mater. Res. **9**, 1028 (1994).
[17] H. P. Ng, X. K. Meng, and A. H. W. Ngan, Scr. Mater. **39**, 1737 (1998).
[18] R. Banerjee, S. Swaminathan, J. M. K. Wiezorek, R. Wheeler, and H. L. Fraser, Metall. Mater. Trans. A **27A**, 2047 (1996).
[19] S. M. Paik, S. Kim, and I. K. Schuller, Phys. Rev. B **43**, 1843 (1991).
[20] K. L. Westra and D. J. Thomson, Thin Solid Films **257**, 15 (1995).
[21] R. Banerjee, X. D. Zhang, S. A. Dregia, and H. L. Fraser, Acta Mater. **47**, 1153 (1999).
[22] *Ternary Alloys—A Comprehensive Compendium of Evaluated Constitutional Data and Phase Diagrams*, edited by G. Petzow and G. Effenberg (VCH, Weinheim, 1988), Vol. 7, p. 434.
[23] K. C. Kao and W. Hwang, *Electrical Transport in Solids* (Pergamon, Oxford, 1981).
[24] I. K. Yoo, S. B. Desu, and J. Xing, Mater. Res. Soc. Symp. Proc. **310**, 165 (1993).
[25] H.-J. Cho, W. Jo, and T. W. Noh, Appl. Phys. Lett. **65**, 1525 (1994).
[26] V. Damodara Das and C. Bahulayan, Thin Solid Films **274**, 55 (1996).
[27] E. D. Macklen, *Thermistors* (Electrochemical, Ayr, Scotland, 1979).
[28] R. F. Bunshah, *Deposition Technologies for Films and Coatings—Developments and Applications* (Noyes, Park Ridge, NJ, 1982), p. 253.
[29] D. A. Hardwick and R. C. Cordi, Mater. Res. Soc. Symp. Proc. **194**, 65 (1990).
[30] E. G. Colgan, M. Nastasi, and J. W. Mayer, J. Appl. Phys. **58**, 4125 (1985).
[31] D. F. Mitchell and M. J. Graham, Surf. Sci. **114**, 546 (1982).
[32] K. L. Chopra, R. Randlett, and R. H. Duff, Philos. Mag. **16**, 211 (1967).
[33] J. C. Slater, J. Chem. Phys. **39**, 3199 (1964).
[34] A. M. James and M. P. Lord, *Macmillan's Chemical and Physical Data* (Macmillan, London, UK, 1992).

Downloaded 05 Nov 2006 to 147.8.21.97. Redistribution subject to AIP license or copyright, see http://jap.aip.org/jap/copyright.jsp